energies

MDPI

Review

An Overview of Solar Photovoltaic Power Smoothing Control Strategies Based on Energy Storage Technology

Mingxuan Mao [1,*], Yuhao Tang [1,2], Jiahan Chen [3], Fuping Ma [4,5], Ziran Li [1], Hongyu Ma [1], Haojin Sun [1], Chengqi Yin [1] and Huanxin Li [6]

[1] School of Automation, Wuxi University, Wuxi 214105, China
[2] School of Automation, Nanjing University of Information Science and Technology, Nanjing 210044, China
[3] Department of Computing, The Hong Kong Polytechnic University, Hong Kong, China
[4] Chengdu Power Supply Company, State Grid Sichuan Electric Power Company, Chengdu 610041, China
[5] School of Electrical Engineering, Chongqing University, Chongqing 400044, China
[6] Physical and Theoretical Chemistry Laboratory, Department of Chemistry, University of Oxford, Oxford OX1 3QZ, UK
* Correspondence: mx_m@cwxu.edu.cn; Tel.: +86-15922927511

Abstract: Countries around the world are actively promoting the low-carbon transformation of the energy system, and renewable energy represented by solar photovoltaic (PV) power generation will occupy a greater proportion of the power system. The power of PV power generation is characterized by randomness and volatility, so an energy storage system (ESS) is needed for smooth control of fluctuating power to improve the quality of electric energy and the stability of the system. First of all, through the comparative analysis of various energy storage technologies, this paper finds that the battery-supercapacitor hybrid energy storage system (HESS) has both steady-state and dynamic response capabilities. Secondly, the power smoothing control strategy comprises centralized control strategies and distributed control strategies, corresponding control algorithms based on filter and optimization, and droop control strategy, respectively. This paper introduces them in turn and analyzes their advantages and disadvantages. Finally, according to the characteristics of the two control strategies, the analysis of the applicable scenarios is given, and it can guide future applications.

Keywords: solar photovoltaic (PV) power; randomness and volatility; energy storage technology; power smoothing control; power quality

Academic Editor: Anastassios M. Stamatelos

Received: 18 December 2024
Revised: 3 February 2025
Accepted: 11 February 2025
Published: 13 February 2025

Citation: Mao, M.; Tang, Y.; Chen, J.; Ma, F.; Li, Z.; Ma, H.; Sun, H.; Yin, C.; Li, H. An Overview of Solar Photovoltaic Power Smoothing Control Strategies Based on Energy Storage Technology. *Energies* **2025**, *18*, 909. https://doi.org/10.3390/en18040909

1. Introduction

Solar energy has attracted more and more attention from people in the past few decades due to the continuous increase in the world's energy demand and people's concern about environmental issues.

Solar energy is abundant energy that is characterized by being extremely clean and inexhaustible [1]. Unlike traditional non-renewable energy sources such as coal, solar energy does not produce any carbon dioxide emissions during use, which is extremely friendly to the environment. Thus, photovoltaic (PV) power generation came into being [2]. However, the PV output power may fluctuate due to the frequent changes in solar irradiance. Because of this, solar energy is vulnerable to uncertainties in the application process. For example, when the weather conditions are poor, such as during cloud cover or in different seasons, the solar irradiance can change greatly. This leads to instability of the PV power, making it difficult to satisfy the energy demand continuously and stably [3,4]. This

uncertainty has brought certain challenges to the wide application of solar energy. It needs to be adjusted and improved through advanced energy storage technology and power smoothing control to enhance the stability and reliability of PV power generation. Thilo Bocklisch [5] summarized the innovation areas of hybrid energy storage systems (HESS), proposed four HESS configurations suitable for distributed PV systems, and proposed a power flow decomposition method based on peak load balancing and double low-pass filtering. A novel smart hybrid energy storage plug-in module system was proposed by Jing et al. [6] aimed at the service life of energy storage devices. It can reduce frequent charge-discharge conversion. Two different operation modes are designed according to the different weather conditions, which can effectively delay the aging of energy storage devices. In Ref. [7], decommissioned lithium iron phosphate batteries from electric vehicles were applied to microgrids. At the same time, grid-connected PV energy storage microgrids were designed based on the load requirements of office buildings, and experimental studies were carried out on their operating performance. The results show that the performance of these decommissioned lithium batteries can satisfy the energy storage requirements. The effect of peak cutting and valley filling is obvious, it can achieve cascade utilization in microgrids. Lei et al. [8] proposed a model predictive control (MPC) based on a power/voltage smoothing strategy. The predicted value in MPC is the equivalent input impedance of the energy storage system (ESS). It can calculate control commands of ESS by using predicted input impedance to achieve better smoothing control. A power smoothing framework based on prediction and adaptive smoothing mechanism was proposed in [9] to avoid arbitrary selection of filtering time constant values and reduce pressure on ESS. In [10], a two-stage adaptive smoothing method based on an artificial potential field was proposed, which can dynamically decompose and distribute power among power grids, batteries, and supercapacitors.

The microgrid is a small power system that is composed of distributed power supply (such as solar PV power generation), energy storage devices, energy conversion devices (such as inverters, rectifiers, etc.), related loads and monitors, protection devices, and another organic whole [11]. It can achieve self-control, protection, and management and can be operated independently or connected to the external power grid [12]. To ensure the stable operation of PV power generation when connected to the microgrid. It is usually necessary to add energy storage devices to maintain the stability of system power [13].

Bullich et al. [14] analyzed the characteristics of each energy storage technology and summarized the most suitable energy storage technology for large-scale photovoltaic power plants. In [15], an integrated review of the current situation and future development of energy storage was made around energy storage technology applied to microgrids. In the context of the mixed use of renewable and non-renewable energy for power generation in today's power grid, Rana et al. [16] emphasized the importance of energy storage systems and proposed a transitional approach to promote the large-scale deployment of energy storage systems in power systems. In [17], aiming at the randomness of PV power generation, the control smoothing technology of different power slopes under three categories was discussed in order to reduce the slope rate of its output power. In this paper, energy storage technology and power smoothing technology are discussed and summarized to provide an application reference.

The research motivation and contributions of this paper can be summarized as follows:

i. This paper reviews some energy storage technologies commonly used in the field of renewable energy. According to the advantages and disadvantages of different energy storage devices, several mainstream HESS are introduced, and a kind of HESS with better comprehensive performance is selected for subsequent analysis to ensure the smooth operation of the microgrid dominated by PV power generation.

ii. To solve the power distribution problem of the system, the power smoothing control strategy based on HESS is discussed. The centralized and distributed power smoothing control strategies are analyzed with emphasis, and the advantages and disadvantages of the control strategies are discussed. The corresponding control strategies can be selected according to the actual requirements.
iii. Combined with the content of this paper, future research prospects on power smoothing control strategy are proposed.

The rest of the paper is organized as follows. Section 2 introduces the comparative analysis of energy storage technology for PV power generation. Section 3 describes the comparative analysis of PV power smoothing control strategies. Section 4 contains the discussion, and Section 5 gives the conclusion.

2. Comparative Analysis of Energy Storage Technology for PV Power Generation

The ESS can compensate when the PV power generation is below the target and store electricity when it is above the target [18]. When the PV output is lower than the target value, the ESS can release the stored electric energy, supplement the power required by the load, and ensure the stability of the power supply. When the PV output is higher than the target value, the excess power can be stored by the ESS for subsequent use when the PV output is insufficient [19]. Such a scheme can effectively deal with the volatility of PV output and improve the utilization efficiency and reliability of PV energy. Energy storage technology has evolved over the centuries and continues to achieve technological breakthroughs. Luo et al. [20] thoroughly discussed the classification, discharge characteristics, and economic benefits of various energy storage devices.

2.1. Single Energy Storage Technology

Battery energy storage (BES) [21,22] converts electrical energy into chemical energy through chemical reactions inside the battery to store it. When electrical energy is needed, chemical energy is converted into electrical output by a reverse reaction. It is worth mentioning that BES is regarded as an ideal energy storage method because of its economic efficiency, strong power balance, and ability to maintain the stability of the power grid.

During troughs of electricity consumption, compressed-air energy storage (CAES) [23] uses excess electrical energy to drive the compressor to compress the air and store it in the gas storage device so that the air stores energy in the form of high-pressure gas. During peaks of electricity consumption, high-pressure air is released and enters the expander to do work, driving the generator to generate electricity. In addition, pumped hydroelectric energy storage (PHES) [24,25] stations usually consist of upper reservoirs, lower reservoirs, and power generation buildings. During troughs of electricity consumption, the excess electric energy is used to pump the water from the lower reservoir to the upper reservoir for storage, and the electric energy is converted into the potential energy of water. During peaks of electricity consumption, water is released from the upper reservoir to the lower reservoir. The generator is driven by the water turbine to generate electricity and convert the potential energy of water into electric energy. Energy storage technologies such as CAES and PHES have greater advantages in support of large-scale energy storage applications [26]. However, these two energy storage methods are limited by environmental and geographical conditions, which makes their development and application face many challenges [27].

The fuel cell (FC) [28,29] converts the chemical energy of a fuel (such as hydrogen) directly into electricity through an electrochemical reaction. In the energy storage process, when there is excess electrical energy, hydrogen can be generated by electrolyzing water and stored. When electricity is needed, the hydrogen is converted again into elec-

trical output by the FC. FC mainly generates water and a small amount of heat, which is more environmentally friendly. However, if the production process of the fuel is not environmentally friendly, the overall environmental benefits will be affected.

Superconducting magnetic energy storage (SMES) [30] uses the zero resistance characteristics of superconductors to pass DC into the superconducting coil and generate a strong magnetic field to store energy. When energy needs to be released, the current in the superconducting coil is directed to the load through a control circuit, thus converting the stored magnetic field energy into an electrical output. It achieves efficient energy conversion and storage by directly storing electrical energy in the magnetic field.

The flywheel energy storage system (FESS) [31–34] is mainly composed of a high-speed rotating flywheel, motor, bearing, and control system. During the charging process, the motor converts electrical energy into mechanical energy, which accelerates the flywheel rotation and stores the energy in the form of kinetic energy. When energy needs to be released, the kinetic energy of the flywheel is converted into electrical energy output by the motor. Despite its unique advantages, its stability and efficiency are greatly affected by mechanical components.

The supercapacitor (SC) stores energy through a double-layer interface formed between electrodes and electrolytes. When the SC is charged, the charge accumulates on the surface of the electrode. Under the action of the electric field, the ions in the electrolyte migrate to the surface of the electrode, forming a double electric layer, thus storing the electrical energy. During discharge, the charge is released from the surface of the electrode. The stored energy is converted into electrical energy output through work performed by the external circuit. As a representative of electrostatic storage, it has attracted much attention for its high recyclability and high density [35].

Table 1 shows the advantages and disadvantages of various energy storage technologies.

Table 1. Comparison of single energy storage technologies.

Energy Storage Technologies	Advantage	Disadvantage
BES [21,22]	• Small size • Flexible installation • High energy density	• Limited life • High maintenance costs
CAES [23]	• Low cost • Large capacity • Long life	• Low energy conversion efficiency • Environmental pollution
PHES [24,25]	• Large capacity • High system efficiency • Long life	• Difficult construction • Limited by environmental conditions
FC [28,29]	• High energy density • Environment friendly	• High cost • Depend on supporting facilities
SMES [30]	• High power density • Low energy loss	• Expensive
FESS [31–34]	• High instantaneous power • Long cycle life	• High cost • Large volume • Low energy density
SC [35]	• High power density • Long cycle life	• Low energy density • High self-discharge rate

In all kinds of energy storage technologies, energy density, and power density are two key indicators [36]. Energy density measures the accumulated energy in the energy storage device of unit volume or mass, while power density reflects the energy transfer rate in the energy storage device of unit volume or mass. Table 2 classifies energy storage technologies according to these two key indicators.

In BES technology, various materials constitute BES with different characteristics. The ternary lithium battery composed of nickel cobalt manganese oxide (NCM) has the

characteristics of high energy density, and the lithium iron phosphate battery composed of $LiFePO_4$ (LFP) has the characteristics of high power density.

Table 2. Classification of energy density and power density.

High Energy Density	High Power Density
BES (NCM)	BES (LFP)
CAES	SMES
PHES	FESS
FC	SC

In addition, energy storage technologies such as CAES, PHES, and FC have a high energy density but a low power density. Therefore, it often faces challenges in power control due to the slow dynamic response. Relatively speaking, energy storage technologies such as SMES, FESS, and SC have high power density and can quickly satisfy high power demands.

2.2. Hybrid Energy Storage Technology

Since there is no energy storage technology that can satisfy the dual requirements of power and energy density at the same time, HESS has emerged. It is designed to improve the overall performance of ESS by combining two or more energy storage technologies into one [36,37]. In particular, the combination of HESS and PV power generation contributes to achieving the optimization and safety of microgrid operation. The positive impact of HESS on PV power generation and microgrid systems was discussed in [38].

In an ideal HESS, one of the energy storage devices is high energy storage (HES), which is used to satisfy long-term energy needs [39]. Another type of storage is high power storage (HPS), which is used to handle power transients and fast load fluctuations. We can obtain a variety of HESS combinations by analyzing different energy storage technologies' HES and HPS characteristics.

In [40], the concepts of utilization factor and hydrogen fuel flow were introduced into the HESS based on the fuel cell as the main and battery as the auxiliary. It enabled FC to achieve the ability to compensate for fast power transients, thus improving the dynamic response capability of HESS. Figure 1 shows its independent microgrid.

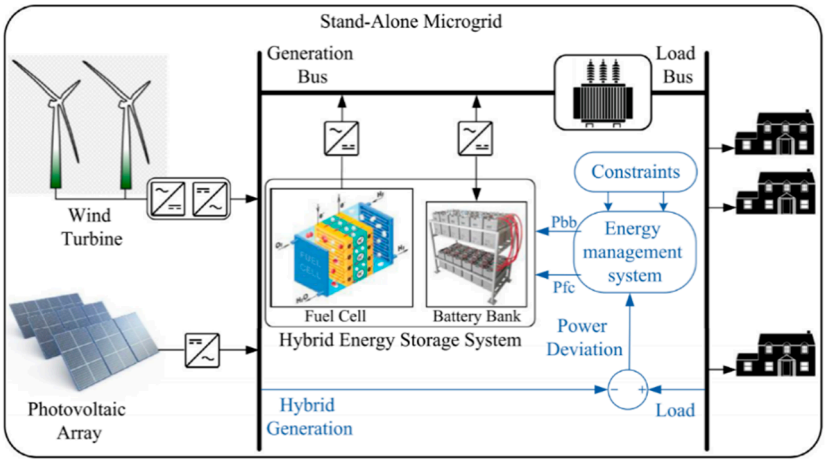

Figure 1. HESS microgrid with FC-Battery [40].

In this independent microgrid system, the load's power needs are met by a combination of wind turbines, PV systems, and FCs. Among them, the battery pack and the FC form a hybrid configuration, whose role is to compensate for fluctuations in instantaneous power. The energy management system prioritizes and regulates the power distribution between the FC and the battery with the help of the droop controller to maintain the main frequency in the preset safe range. Both the wind turbine and the PV system operate in maximum

power point tracking mode, with the former connected to the generation bus via an AC-AC converter and the latter connected to it via a DC-AC converter. At the same time, the FC and battery pack are also connected to the power generation bus via a DC-AC converter. The load bus is connected with the power generation bus by the transformer, so as to supply power to the load.

The output voltage of the solid oxide fuel cell system is:

$$V = N_0\left(E_0 + \frac{RT}{2F}\left[Ln\left(\frac{p_{H_2}p_{O_2}^{0.5}}{p_{H_2O}}\right)\right] - rI_{FC}\right) \quad (1)$$

where N_0 is number of cells in series in the stack, Eo is ideal standard potential, R is universal gas constant, T is absolute temperature, F is Faradays constant, p_{H_2} is partial pressure of hydrogen, $p_{O_2}^{0.5}$ is partial pressure of oxygen, p_{H_2O} is partial pressure of water, r is ohmic loss and I_{FC} is fuel cell current.

The energy state of the battery bank is as follows:

$$E_{BB}(t) = E_{BB}(t-1) + \eta_{BB} \times P_{BB}(t) \times \Delta t \quad (2)$$

where P_{BB} is the charge/discharge power of the battery bank during a time interval Δt and η_{BB} is the charge/discharge efficiency of the battery bank [40].

The Flywheel-Battery HESS can enable smooth charging and discharging of batteries. In addition, the flywheel can filter out harmful effects, reduce battery damage, and extend battery life. Yang et al. [41] proposed a new fusion deconvolution method. It can conduct a reliability analysis of the Flywheel-Battery HESS to avoid mechanical failures when the flywheel speed is sky-high. Figure 2 shows its schematic diagram.

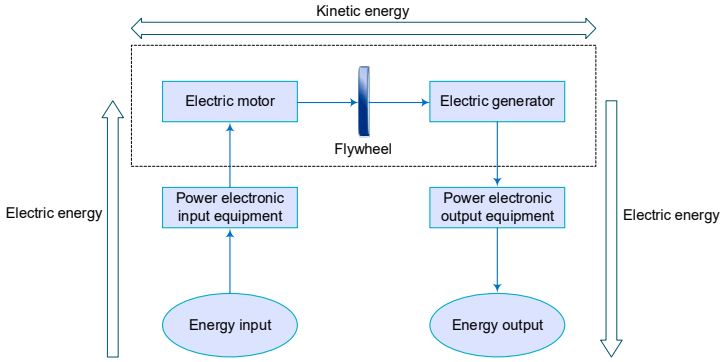

Figure 2. The theory of Flywheel-Battery HESS [41].

The flywheel is an integrated motor/generator system with two operating modes: one is a charging mode, which uses battery power to drive the flywheel motor at high speed, with a speed of 20,000–100,000 revolutions per minute, so that kinetic energy can be stored in the flywheel; second is the discharge mode, which releases the stored kinetic energy of the flywheel by driving the flywheel generator until the flywheel speed drops to zero. In this process, kinetic energy can be converted into electricity needed by the battery. It is worth mentioning that in the process of electromechanical energy exchange between the flywheel and the battery, harmful components can be effectively filtered out, and then the charge and discharge process of the battery becomes smooth, so as to effectively protect the battery.

The kinetic energy E stored by the flywheel can be expressed as:

$$E = \frac{1}{2}J\omega^2 = \frac{1}{2}mr^2\omega^2 \quad (3)$$

where J represents a moment of inertia, ω is the angular velocity of the flywheel, m is the mass of the cylinder and r represents the radius [42].

A new semi-active Battery-SC hybrid scheme with variable voltage control for firm frequency response services was proposed by Li et al. [43]. It improves the utilization rate of SC, at the same time reduces the cost of the converter. Figure 3 shows the configuration of HESS.

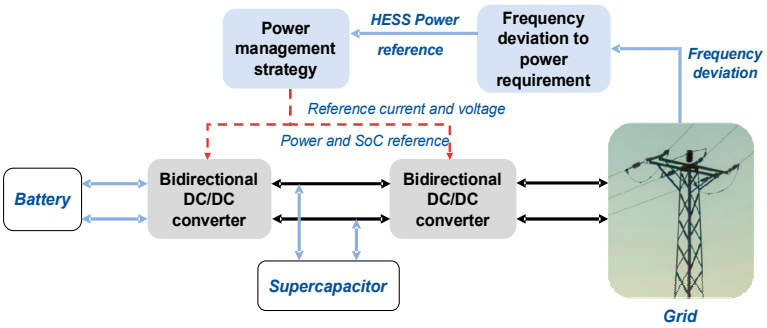

Figure 3. Battery-SC hybrid energy system configuration for firm frequency response.

In power systems, to mitigate the frequency fluctuations with the firm frequency response envelope, HESS units are connected to the main grid via power converters. The battery is connected to the DC bus through the DC-DC converter, and the SC is directly connected to the DC bus, so that the voltage of the SC will change with the change of the DC bus voltage. For the traditional power control mode in the power grid, the DC bus voltage needs to be maintained at a certain value or fluctuate near a constant value. However, this may make the utilization of SC very low, in which case the SC only plays the role of ordinary filters. Therefore, in order to protect the battery from the adverse effects of instantaneous power fluctuations, and to ensure that the SC is within the range of efficient operation. It is necessary to control the DC bus voltage on the semi-active method of the SC, so that it can fluctuate in a deeper range.

The equation of SC is described in the following equation:

$$V_{\mathrm{sc}} = \frac{1}{C^*} \int \left(\left(1 + \frac{R_{\mathrm{esr}}}{R_{\mathrm{leak}}} \right) I_{\mathrm{sc}} - \frac{V_{\mathrm{sc}}}{R_{\mathrm{leak}}} \right) dt + I_{\mathrm{sc}} R_{\mathrm{esr}} \tag{4}$$

where R_{leak} is the leakage resistance, R_{esr} is the series resistance, and C^* is the effective capacitance of SC.

The battery capacity model can be described as shown in the following equation:

$$\mathrm{Soc}(t+1) = \begin{cases} Soc(k) - \eta_C \frac{T_S}{Q} I_{\mathrm{Batt}}(k) : I_{\mathrm{Batt}}(k) \leq 0 \\ Soc(k) - \frac{T_S}{\eta_D Q} I_{\mathrm{Batt}}(k) : I_{\mathrm{Batt}}(k) \geq 0 \end{cases} \tag{5}$$

where T_S is the sampling time, η_C and η_D define the charge/discharge efficiency of the battery. I_{Batt} represents the battery charge/discharge. The positive value implies that the battery supplies energy while the negative sign implies the battery absorbs energy [43].

In [44], a new SMES-Battery HESS cascade topology construction was proposed. It not only avoids the use of droop control but also retains the advantages of traditional HESS schemes such as fast response speed and large energy capacity. Thus, the transient problem during the switching between the battery and SMES is solved. Figure 4 shows its cascade structure chart.

The system mainly consists of two converters (H1 and H2), an SMES coil, and a battery. The converters H1 and H2 consist of two controllable IGBT switches and two diodes, namely S1–S4 and Q1–Q4, respectively. SMES are embedded between the joints A1 and

B2 of the two converters. The connection of B1 and A2 is used for current continuity. The battery is connected to the H2 output ports M2 and N2. H1 output ports M1 and N1 connect to the DC bus on the battery side. Two capacitors C1 and C2 are used for filtering. In industrial applications, two additional switches (BP1 and BP2) are added to the structure in order to enable the S-B HESS to continue working when one of the energy storage units is damaged or stopped. When the SMES fails, BP1 will be activated, and S-B HESS will work as a single battery energy storage device. In contrast, when the battery fails to function properly and the system works in single-SMES mode, BP2 will be activated to isolate the battery part.

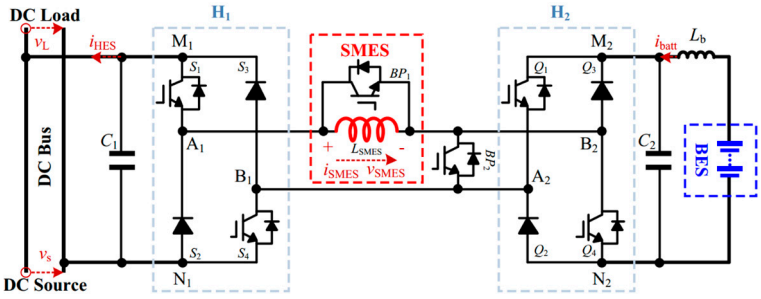

Figure 4. Structure of the cascaded SMES-Battery HESS [44].

The terms i_{batt} and i_{HES} represent the output current of the battery and the S-B HESS, respectively. i_{SMES} is the SMES operating current. The load side voltage and the source side voltage are defined as v_L and v_s, respectively. The inductance of the SMES is L_{SMES}, I_{SMES} is the SMES rated current and the SMES withstanding voltage is defined as v_{SMES} [44].

The stored energy (E_{SMES0}) in the SMES available for compensation can be expressed as:

$$E_{SMES0} = \frac{1}{2} L_{SMES} I_{SMES0}^2 \tag{6}$$

Xu et al. [45] proposed a terminal sliding mode control strategy for HESS. This strategy is based on the adaptive law of projection operators. The goal is to supply power to the load in time. It can track the current of FC, battery, and SC well, and then obtain a stable DC bus voltage. Figure 5 shows its circuit topology diagram.

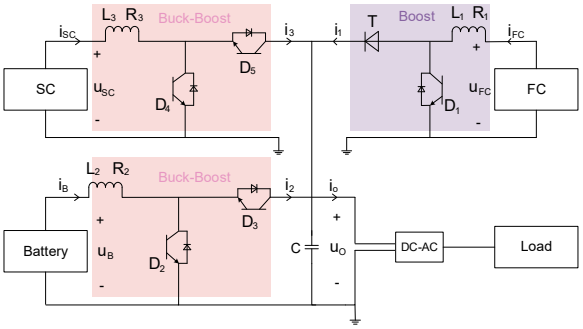

Figure 5. Circuit topology of the FC-Battery-SC HESS.

HESS uses a boost converter, two buck converters, and an additional control circuit. The control circuit can achieve the optimal power distribution under the guidance of the strategy. FC and battery are both major energy components, which are capable of operating under different load power conditions. At the same time, batteries and SCs are energy storage devices. When the FC is operating in low efficiency or failure mode, or when the load is charging the system, the battery is the dominant part. Due to the unique physical properties of SC, it can obtain peak power that FC and battery cannot provide. The boost

converter consists of an insulated gate bipolar transistor (IGBT), a diode T, a filter capacitor C, and a high frequency inductor L1. The bidirectional DC-DC converter consists of two IGBTs and a high-frequency filter inductor. The current output from the boost converter and buck-boost converter flows through the capacitor and is then connected to the DC-AC converter, where the power is finally transferred to the load.

The operation model of FC can be expressed as:

$$\frac{di_{FC}}{dt} = -\frac{R_1}{L_1} i_{FC} + \frac{1}{L_1} u_{FC} - \frac{1 - m_1}{L_1} u_O \tag{7}$$

where the symbol m_1 means the duty cycle of the IGBT D_1, which varies from 0 to 1.

The operating model of the battery can be expressed as follows:

$$\frac{di_B}{dt} = -\frac{R_2}{L_2} i_B + \frac{1}{L_2} u_B - \frac{m_{23}}{L_2} u_O \tag{8}$$

$$m_{23} = \begin{cases} 1 - m_2 & i_B^* > 0 \\ m_3 & i_B^* < 0 \end{cases} \tag{9}$$

where i_B^* represents the battery current reference, m_2 and m_3 means the duty cycle of the IGBT D_2 and D_3, respectively.

The operation model of SC can be expressed as:

$$\frac{di_{SC}}{dt} = -\frac{R_3}{L_3} i_{SC} + \frac{1}{L_3} u_{SC} - \frac{m_{45}}{L_3} u_O \tag{10}$$

$$m_{45} = \begin{cases} 1 - m_4 & i_{SC}^* > 0 \\ m_5 & i_{SC}^* < 0 \end{cases} \tag{11}$$

where i_{SC}^* means the current reference of SC, m_4 and m_5 means the duty cycle of the IGBT D_4 and D_5, respectively [45].

Common HESS combinations are shown in Figure 6.

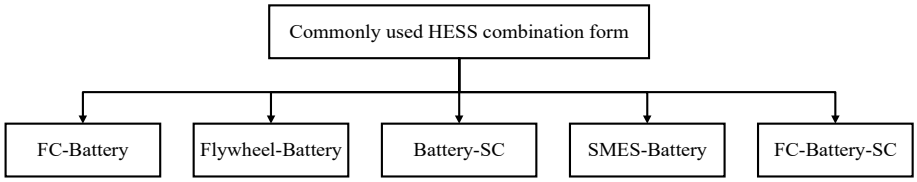

Figure 6. HESS combinations.

By comprehensively considering the energy storage capacity demand, occupied space, economic cost, and other factors. Selecting the appropriate HESS combination can effectively deal with intermittency [46], poor power quality [47], poor stability [48], frequency instability [49], DC bus voltage fluctuation [50], and other technical problems existing in PV power generation.

Among various HESS, the Battery-SC HESS [51,52] has been widely concerned and applied because it takes into account both steady-state and dynamic response capabilities. The high energy density of the battery can satisfy the power demand required by the system. However its dynamic response speed is slow, and it is difficult to solve the high-frequency components of power fluctuation [53]. SC focuses on compensating transient power fluctuations due to its own high power density and fast dynamic response speed. However, its low energy density characteristic makes it unable to cope with low-frequency components of power fluctuations. The HESS formed by the two can complement each other's advantages and satisfy the needs of PV power smooth control [54]. According to

the different advantages of battery and SC, the types of power demand distributed in HESS also have different focuses. How to achieve effective fluctuating power distribution is a huge problem that needs to be solved [55].

3. Comparative Analysis of PV Power Smoothing Control Strategies

The PV power signal contains complex frequency components. Among them, there is key frequency information that has an important influence on power characteristics. The low-frequency component carries the main trend characteristics of PV power, while the high-frequency component is often mixed with fluctuation information caused by factors such as rapid changes in cloud cover and ambient light interference [56]. In recent years, researchers have proposed various control strategies to achieve power distribution between HESS, so as to achieve smooth output power control. According to the system structure, these control strategies can be divided into two categories: centralized control strategy and distributed control strategy.

3.1. Centralized Power Smoothing Control Strategy

The centralized control strategy uses a central controller to sample the PV power. Through various signal processing technologies, the low-frequency and high-frequency components of the fluctuating power are extracted, and the output command is sent to the HESS through communication technology. The centralized control strategy can be further subdivided into filter-based control algorithms and optimization-based control algorithms [57].

In the filter-based approach, the system's power fluctuation response requirements are divided into high-frequency components and low-frequency components by using filters. They are responded to by SC and battery, respectively. The commonly used filtering technology mainly includes high/low pass filter, wavelet transform, empirical mode decomposition (EMD), moving average, and so on.

The low pass filter (LPF) can help distinguish high-frequency fluctuations and low-frequency useful signals. And transmit the information of high-frequency fluctuations signals to the controller of the ESS so that the ESS can carry out charge and discharge control more accurately [58]. In [59], an improved LPF controller is proposed. The power direction control strategy eliminates unbeneficial power exchange, reduces the capacity of HESS, and improves the unnecessary energy exchange problem between storage elements due to time delay caused by phase lag in LPF. Thus, the HESS round-trip energy efficiency has been improved. The block diagram of the conventional LPF controller is shown in Figure 7. Roy et al. [60] used the LPF to distribute power between the battery and the SC. And carried on an economic comparison of HESS with different time constants of LPF. In addition, the state of charge (SOC) control algorithm is added to maintain the SOC of energy storage within a certain range. As a result, the service life of the storage energy is extended, and a cost-effective ESS is developed.

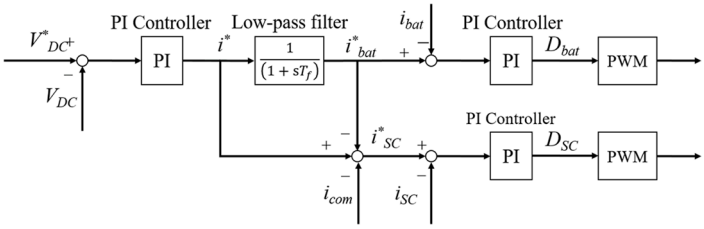

Figure 7. Block diagram of conventional LPF controller [59].

In a traditional LPF controller, the DC grid voltage V_{DC} is first compared to the reference voltage V^*_{DC}, and the error is provided to the proportional integration (PI) controller.

The PI controller generates the required total HESS current i^*. Then i^* is divided into a low frequency reference current i^*_{bat} (for batteries) and a high frequency reference current i^*_{SC} (for SC). Therefore, through the current reference, LPF allocates the reference power of energy storage devices to:

$$\begin{cases} P_{bat}(s) = P_{HESS}(s) \cdot \frac{1}{1+sT_f} \\ P_{SC}(s) = P_{HESS}(s) - P_{bat}(s) \end{cases} \quad (12)$$

where T_f is the time constant of the LPF [59].

The reference current i^*_{bat} is then compared with the battery current i_{bat}. This error is fed to the PI controller to generate the duty cycle D_{bat}. Based on the duty cycle D_{bat}, the pulse width modulation (PWM) generator controls the battery's DC-DC converter. Due to the SC's high self-discharge rate, the energy stored in the SC decays over time, requiring an i_{com} to be added to compensate. The SC reference current i^*_{SC} is also compared with the SC current i_{SC}, and the error is passed to the PI controller to generate the duty cycle D_{SC}. The PWM generator controls the SC's DC/DC converter via duty cycle D_{SC}.

The wavelet transform can be used to isolate the low-frequency component from the high-frequency component [61]. At the same time, the wavelet transform also gives a concept of the storage system capacity required to suppress the high-frequency component, so it is an effective method to smooth the PV fluctuation power [62]. A power adaptive smoothing suppression method for the point of common coupling with distributed PV energy storage based on empirical wavelet transform was proposed in [63]. The PV power is decomposed adaptively by empirical wavelet transform, and the HESS power is distributed according to the response capacity of different energy storage components. In addition, an active power compensation SOC control strategy is provided for HESS SOC. The structure of the wavelet filter bank is shown in Figure 8.

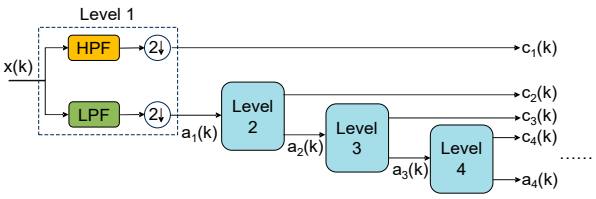

Figure 8. Wavelet filter bank structure.

EMD can decompose the PV power signal into multiple intrinsic mode functions (IMF) and a residual component. For example, the power of short-time sharp changes caused by rapid cloud movement is decomposed into high-frequency IMF, while the power of slow changes caused by seasonal changes may appear in low-frequency IMF or residual components. We can formulate corresponding power smoothing strategies for different frequencies' IMF based on the results of EMD decomposition [64]. Zheng et al. [65] proposed a hybrid energy storage smooth output fluctuation control strategy based on considering PV dual evaluation indexes. The EMD will be continued again when there are abnormal signals in the process of ensemble EMD. Then, the final modal component will be obtained by removing the pseudo-component. We can reconstruct the power based on the grey relational degree, and the smooth power output fluctuation instructions for SC and battery will be obtained. Volatility and smoothness are two evaluation indexes, according to different time scales, and moving average filtering is used as the instruction. The battery pack (5 min scale) and SC pack (1 min scale) in hybrid energy storage coordinate and control PV smoothing output fluctuation. The EMD steps are shown in Figure 9. Among them, the two constraints of the IMF are:

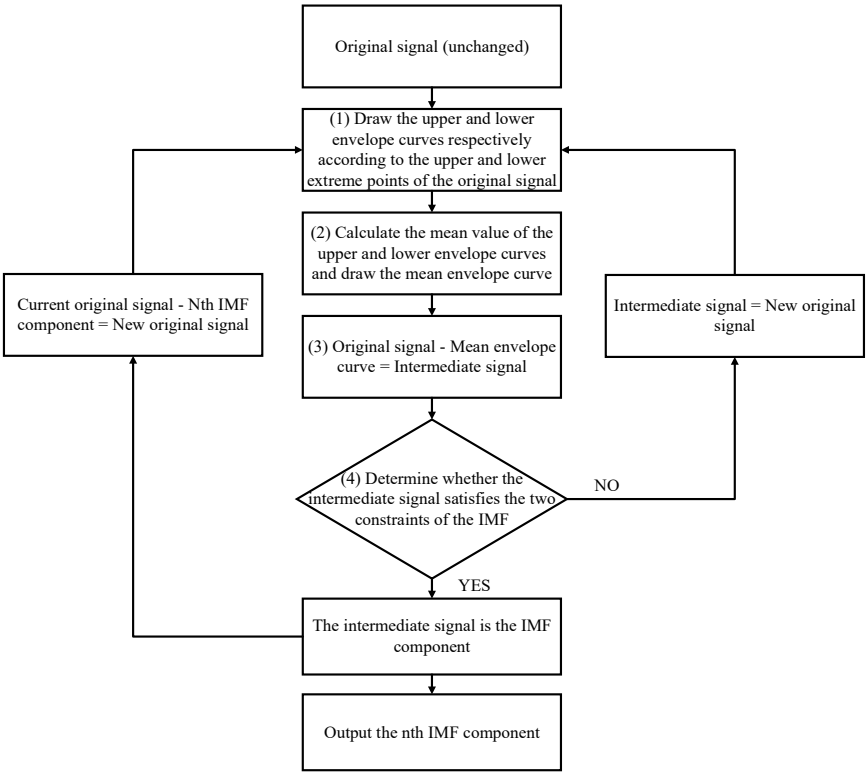

Figure 9. The flow diagram of EMD.

(1) The number of extreme and zero points must be equal or differ by no more than one throughout the data segment.

(2) At any time, the average value of the upper envelope curve formed by the local maximum point and the lower envelope curve formed by the local minimum point is zero; that is, the upper and lower envelope curves are locally symmetric concerning the time axis.

The basic principle of the moving average method is to average a series of data (such as a PV power data series) according to a certain window size [66]. The ESS can reasonably arrange charge and discharge according to the power change trend after the moving average to achieve smooth control of PV power [67]. A power distribution method based on multiple moving average filtering is proposed in [68]. First, the minimum total power instruction of HESS satisfying the requirements of suppression is obtained, and then the respective power instruction of the battery and SC is obtained through multiple moving average filtering. At the same time, the Pearson correlation coefficient is introduced to judge the number of filters and the size of the sliding window. The volume of HESS is determined according to the power distribution results. Finally, the life cycle quantization model of the battery is established to limit the mode aliasing and reduce the comprehensive cost of HESS. The moving average method is shown in Figure 10.

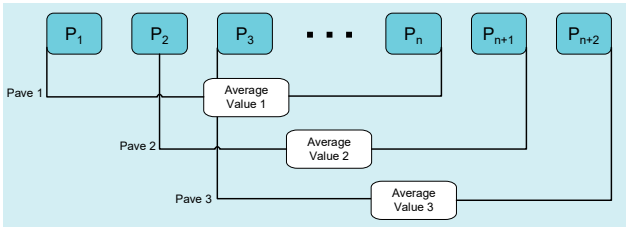

Figure 10. Moving average method.

Figure 11 shows the structure of a centralized power smoothing control strategy based on filters.

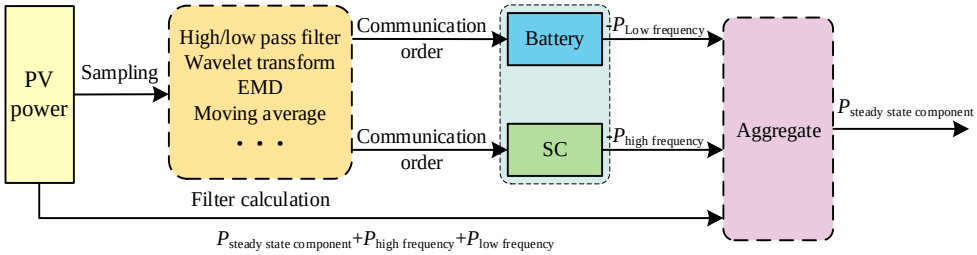

Figure 11. Schematic diagram of centralized power smoothing control strategy based on filter.

In the optimization-based control algorithm, the power distribution problem inside the HESS is decomposed into sub-problems under different control strategies by using various optimization control algorithms. The corresponding control logic deals with these sub-problems, respectively [69,70]. The commonly used optimization-based control algorithms mainly include MPC, artificial neural network (ANN), fuzzy logic control, and so on.

MPC uses system models to predict fluctuations in PV power. Through the analysis of historical solar radiation data, meteorological information, and the current operating state of the PV system, a dynamic model between PV power and related influencing factors is established [71]. Based on this model, MPC can predict the changing trend of PV power in a short time in advance, including the peak value, valley value, and change rate of power. It can provide a basis for subsequent smooth control [72]. Hredzak et al. [73] proposed an MPC strategy applied to HESS. The battery and SC are connected to the DC bus through a bidirectional DC/DC converter. The model prediction controller, respectively, provides a modulation index to the battery and the SC in HESS to adjust the shared load power between them. At the same time, it can achieve the distribution effect that the battery responds to the change of slow load current, and the SC responds to the change of fast load current by setting a higher cost for changes in battery current. In [74], an MPC strategy for achieving optimal economic scheduling in microgrids was proposed, which involves multiple energy storage forms such as battery, FC, and SC. In this system, various energy storage devices are connected to the AC power grid through inverters. The MPC strategy also considers the following factors: the system operating cost, energy storage component degradation cost, and operating constraints. The system achieves the optimal power allocation of economic cost [75]. The schematic diagram of MPC is shown in Figure 12.

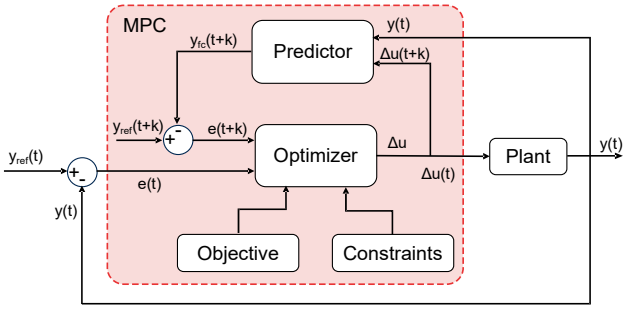

Figure 12. Basic principle of the MPC.

The ANN is a computational model that mimics the structure and function of biological neural networks. It consists of a large number of neurons connected to each other, and neurons are the basic processing units. These neurons are arranged in layers, usually including input layers, hidden layers, and output layers. [76]. The ANN can predict changes in PV power and can generate appropriate control strategies based on the predicted power

changes. If the power is predicted to rise, the inverter can be controlled to adjust the power output, or the ESS can be arranged to charge to absorb the excess power. If the power is predicted to decline, the ESS can be arranged to discharge to maintain the stability of the power output. In [77], a model-free energy management controller based on HESS is proposed, which is achieved by ANN with dynamic programming technology. The dynamic programming technique is used to solve the predefined cost function and provide the duty cycle after optimization to ANN as training data. After training, the ANN can operate alone. It can adjust the control signal of the multi-source inverter to satisfy the required load current and achieve the allocation of performance. The ANN architecture is shown in Figure 13.

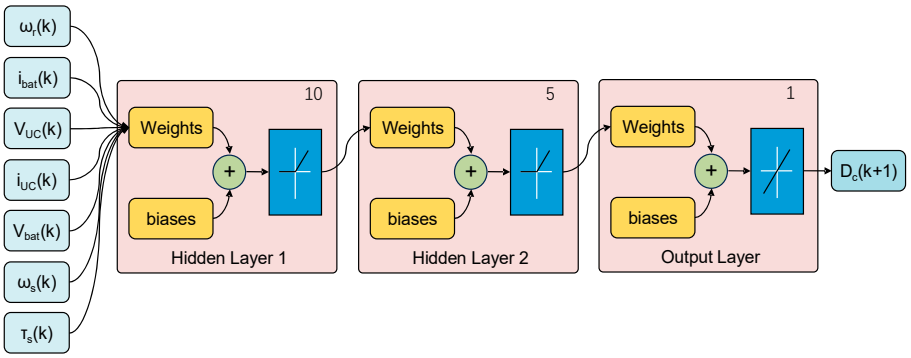

Figure 13. ANN designed architecture.

The core of fuzzy logic control is the fuzzy set and fuzzy rule. Unlike traditional sets, in the fuzzy set, the degree of membership that elements to the set is a value between 0 and 1, and it is defined by the membership function. Fuzzy rules usually take the form of "If-Then" to describe the fuzzy relationship between input and output [78]. For example, "If the temperature is high and the light is strong, then the power output is high". In PV devices with ESS, fuzzy logic control can be used to coordinate the operation of PV and ESS. Fuzzy rules can be formulated according to the PV power and the SOC of the ESS. If the PV power is too high and the ESS is not full, then the ESS can charge to absorb the excess power and achieve a better power smoothing effect. Cohen et al. [79] proposed a control scheme composed of four PI controllers and one fuzzy logic controller for HESS with pulse load, and the HESS adopts a semi-active topology. The battery is connected to the DC bus through a bidirectional DC/DC converter, while the SC is directly connected to the DC bus. So, the battery can be actively controlled. The proposed fuzzy logic controller uses predefined fuzzy rules to enable or disable the corresponding PI controller. It can simultaneously achieve the DC bus voltage regulation and battery output minimization when the pulse load is accessed. A multi-mode fuzzy logic controller for HESS power distribution used in PV systems was proposed in [80]. Through the collaborative work of the three fuzzy logic controller operating modes, it can achieve mismatch power compensation, hybrid energy storage power distribution, and the restoration function of SC's SOC in both short-term and long-term use scenarios. The structure of the fuzzy controller is shown in Figure 14.

Since implementing the above control strategies requires a centralized controller, they are classified as centralized control strategies. To ensure good control performance, it is necessary to ensure accurate and timely communication between the central controller and the local controller. However, the inevitable communication delay and single point of failure will deteriorate the performance of the centralized control strategy and reduce the reliability of the microgrid system [81].

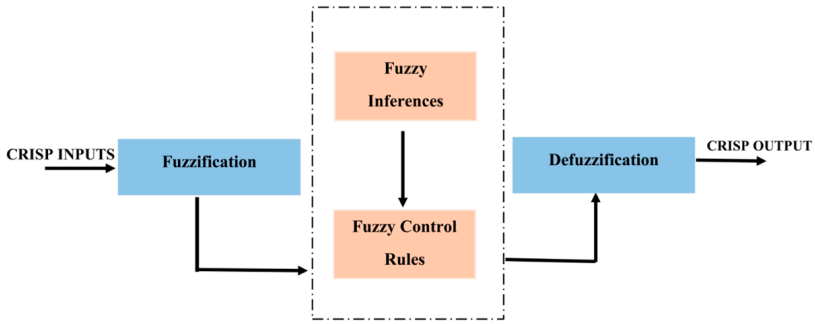

Figure 14. Block diagram of fuzzy controller [78].

3.2. Distributed Power Smoothing Control Strategy

The basic principle of droop control is similar to the traditional synchronous generator [82]. In the AC power system, droop control mainly involves two kinds of droop characteristic relation: power-frequency and voltage-reactive power. When the load in the system changes or the output power of the distributed power supply changes due to external factors. The system will automatically adjust the power output according to the preset droop characteristics based on the detected frequency and voltage changes [83].

Unlike centralized control strategies, distributed control strategies based on droop control only rely on local information. It can avoid communication requirements among controllers and reduce the burden of communication and computation in the system. By adjusting the droop coefficient, the power distribution among distributed power supply can be flexibly controlled.

V-I droop control takes voltage as the main control variable, and the current will adjust according to the change in voltage. It is a feedback control strategy. That is, when the voltage changes, the current will change according to the predetermined droop characteristics. In the V-I droop control strategy, the virtual resistor droop controller and virtual capacitor droop controller are applied to the battery and the SC, respectively, to automatically achieve the distribution of power between the two. The V-I virtual impedance droop control structure is shown in Figure 15. In [84], the SOC recovery loop is added to the control of the SC, which helps to automatically restore the SC's SOC and enable it can run continuously. Xu et al. [85] discussed the influence of line impedance on power distribution and carried out the corresponding controller loop design. In [86], voltage droop caused by the droop coefficient is recovered and the control strategy is extended to multiple HESS. For energy storage unit clusters with a high slow variation rate, an integral droop control strategy was proposed by Lin et al. [87]. The strategy of coordinated control with the traditional voltage-power droop control strategy contributes to carrying out the distribution of transient power in a single HESS in a decentralized manner. Zhang et al. [88] used a virtual impedance loop to add virtual resistors and virtual capacitors in series between the converter and the DC bus. It can ensure plug-and-play characteristics while decoupling the power flow among SC and other distributed generation units.

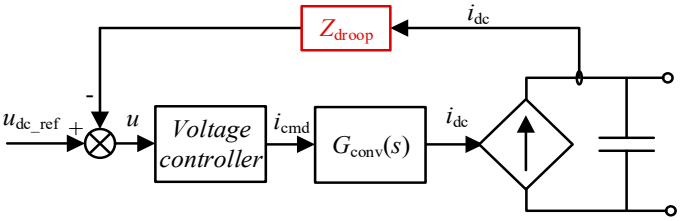

Figure 15. Schematic diagram of V-I virtual impedance droop control strategy.

The voltage bias u can be expressed as:

$$u = u_{dc\_ref} - Z_{droop} i_{dc} \tag{13}$$

where u_{dc_ref} is the DC reference voltage, Z_{droop} is the virtual impedance, i_{dc} is the actual output DC current, and $G_{conv}(s)$ is the transfer function of the converter. After processing, the error signal u is converted into current command i_{cmd}, which prompts the transformer and other links to change the output current according to the current voltage deviation, so as to adjust the output voltage to the desired state [89].

Similar to the V-I droop control, the I-V droop control takes current as the main control variable, and the voltage will adjust according to the change in current. When the current changes, the voltage will change according to the predetermined droop characteristics. Therefore, I-V droop control is also a widely used control method in microgrid applications. It takes DC bus voltage as a feedback signal to achieve accurate current sharing. Figure 16 shows the I-V virtual impedance droop control structure. Wang et al. [90] used virtual impedance instead of constant droop coefficient in I-V droop control to achieve dynamic power sharing between battery and SC. In [91], let the battery and the SC absorb low-frequency and high-frequency power fluctuations, respectively, by refining the virtual output impedance of ESS in the frequency domain. The coordination of time scale and power scale in distributed microgrid systems can be achieved. A pattern adaptive decentralized control strategy was proposed by Gu et al. [92]. It can achieve power sharing between different power supplies through the DC bus voltage signal, and establish the operation mode of the microgrid, in which the control mode can achieve seamless conversion. A distributed power distribution strategy based on power buffers that can dynamically form multiple HESS was proposed in [93]. The power buffer and SC can split the power mismatch into low-frequency and high-frequency parts by adopting the modified I-V droop control strategy. The low frequency is compensated by the battery according to the respective SOC, and the high frequency is directly handled by the SC. This new scheme further eliminates the voltage deviation of the DC bus.

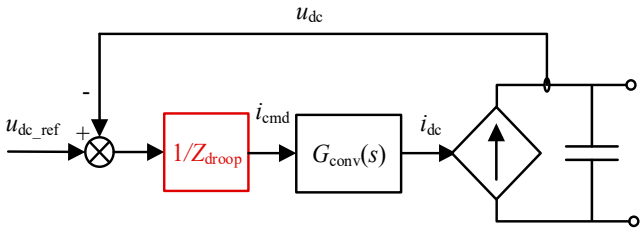

Figure 16. Schematic diagram of I-V virtual impedance droop control strategy.

The output current command i_{cmd} can be expressed as:

$$i_{cmd} = (u_{dc\_ref} - u_{dc}) / Z_{droop} \tag{14}$$

where u_{dc_ref} is the DC reference voltage, u_{dc} is the actual DC voltage, and Z_{droop} is the virtual impedance (for converters with a Battery, it can be adjusted with the virtual inductance $Z_{droop} = sL_v$ droop controller; for converters with SC, it can be adjusted with the virtual resistance $Z_{droop} = R_v$ droop controller), $G_{conv}(s)$ is the transfer function of the converter and i_{dc} is the actual output DC current. Due to the addition of virtual impedance, the droop characteristics of the system can be changed by adjusting the value of virtual impedance, and the power distribution and dynamic performance of the system can be adjusted [90].

Furthermore, Gao et al. [89] conducted a comparative study on I-V and V-I droop control. It focuses on steady-state power-sharing performance and stability. By deducing the system's output impedance and corresponding dynamic characteristics, a generalized

analytical impedance model is proposed to explore the system's stability. Wang et al. [94] compared the dynamic response performance of I-V droop control and V-I droop control by establishing a state-space model and proved the advantages of I-V droop control in dynamic response. In addition, an adaptive PI controller is proposed to improve the dynamic response while ensuring good steady-state performance. Figure 17 shows the adaptive PI controller architecture.

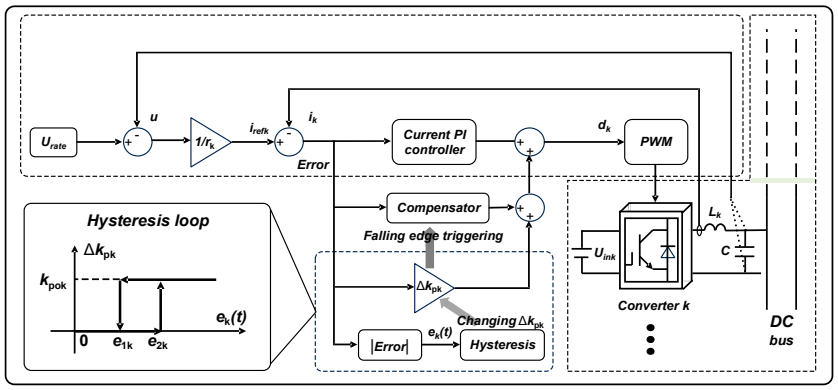

Figure 17. Adaptive PI controller based on droop control.

In Figure 17, U_{rate} is the rated voltage, which is subtracted from the feedback signal u, and the difference value gets the reference current i_{refk} through link $1/r_k$, where r_k is the droop coefficient. The comparison of the reference current i_{refk} with the actual current i_k generates an error signal that is fed into the current PI controller. The PI controller outputs d_k, which is used to control the PWM module and then adjust the working state of the converter.

Let $e_k(t)$ be the absolute error between the current reference and the average inductor current of the kth converter, then

$$e_k(t) = \left| -\frac{1}{r_k} u_d(t) - i_{dk}(t) \right| \tag{15}$$

When $e_k(t)$ changes, Δk_{pk} also changes:

$$\begin{cases} \Delta k_{pk} = 0 & e_k(t) < e_{1k} \\ \Delta k_{pk} = k_{pok} & e_k(t) > e_{2k} \\ \Delta k_{pk} \text{is kept unchanging} & e_{1k} < e_k(t) < e_{2k} \end{cases} \tag{16}$$

where Δk_{pk} means the variation of proportional term of the kth converter, and Δk_{pk} needs to be increased to k_{pok} to improve the response speed when the absolute error increases to e_{2k}. As the absolute error is less than e_{1k}, Δk_{pk} returns to zero to eliminate the error rapidly and guarantee good stead-state performance.

However, since the difference between the average inductor current and current reference is not always zero at the very beginning of Δk_{pk} restoring to zero, the output duty ratio of the PI controller will change back at the falling edge of Δk_{pk} to induce that the output current returns back, which can increase Δk_{pk} to k_{pok} again. Since the above processes can take place repeatedly, fluctuations of currents will be induced, and the dynamic can be weaker.

In order to solve this problem, an improved method for this adaptive PI controller is proposed. At the very beginning of Δk_{pk} restoring back, the output duty ratio needs to be

constant to hold the inductor current, so a compensation term needs to be added to the output duty ratio at the falling edge of Δk_{pk}, which can be computed as

$$d_{cpk} = k_{pok}[i_{drefk}(t) - i_{dk}(t)] \quad (17)$$

where d_{cpk} is the compensation value for the kth converter. Due to this improvement, the repeated fluctuations of currents can be avoided, and the voltage and current can smoothly transition from the dynamic process to the steady state. Thus, the dynamic response performances can be improved by the adaptive PI controller, and the steady characteristics can be guaranteed simultaneously [94].

4. Discussion and Outlook

The PV power smoothing control strategy can be divided into centralized power smoothing control strategy and distributed power smoothing control strategy.

A centralized control strategy collects information from the system's various parts through a central controller. According to this information, corresponding control decisions are made to achieve power smoothing control. Through the whole system's unified management and control by the central controller. The system can uniformly allocate and dispatch power according to the overall operation target and can reasonably arrange the charging and discharging time and power size according to the energy storage state and PV power fluctuations to avoid resource waste. But at the same time, it is highly dependent on the centralized controller. Once the controller fails, it may lead to the failure of the whole power smoothing control system and cause a great impact on the power grid. In addition, the centralized controller needs to collect and process a large amount of information from the system's various parts, which puts high requirements on communication systems and computing power [95]. A control strategy based on MPC was proposed in [96], which designed a centralized controller based on MPC's current tracking technology. The control scheme adopts complex model prediction current control for DC/DC bidirectional converter and adopts model prediction power and voltage combination control for bidirectional interconnect converter. Efficient power distribution is achieved for power grid-interactive PV microgrids with HESS. Sun et al. [97] designed a centralized microgrid control system and proposed an auxiliary slack bus power control method based on closed-loop feedback and first-order filtering. The method can not only alleviate power fluctuations to satisfy smooth control but also compensate for the feeder line loss ignored in the scheduling algorithm.

The distributed control strategy distributes the control to each part of the system, and each part is controlled by its local controller. Because control functions are distributed across multiple local controllers, even if one part fails, the others can continue to work. Thus, the reliability of the system is developed. Moreover, because there is no need for complex communication and centralized processing, the local controller can directly obtain the local device information. The system can quickly respond to the output power change [98]. However, because the control is distributed, different local controllers may make different power adjustment choices according to their information, resulting in the situation of local optimal but global non-optimal. So, the overall power smoothing effect is not as good as the centralized control. In [99], a distributed control strategy based on improved DC bus signaling was proposed for PV power generation systems with battery energy storage. It considers the power balance of the system under extreme conditions and discusses the control methods of the DC/DC converter, battery converter, and grid-connected converter. A power smoothing control strategy for distributed renewable energy power generation based on SC was proposed in [100]. The power smoothing controller generates a power reference for the DC/DC converter, which uses sliding mode technology to achieve power tracking control. The scheme allows the cut-off smoothing frequency to be specified while

guaranteeing the optimal charging state of the ESS without the need for additional filters or predictive algorithms.

Droop control does not require complex communication systems to achieve coordinated operation between distributed power sources [101]. It can be based on the voltage and frequency information measured locally and automatically adjust the output power of the distributed power supply according to the preset droop characteristic curve. Therefore, droop control plays an indispensable role in the distributed power smoothing control strategy.

The V-I droop control can adjust the output current according to the voltage change of each power supply to achieve a reasonable distribution of power among each power supply. In an ESS composed of multiple batteries, the voltage of a certain battery decreases due to aging or other factors. The output current of the battery will increase accordingly through V-I droop control so that it can share the load power with other batteries to avoid the overload of a certain battery.

The I-V droop control mainly affects power distribution indirectly through voltage adjustment caused by current change. If the droop coefficient is set improperly or the current change in the system is too drastic, the voltage fluctuation may be large. Then, the stability of the system will be affected. Especially in some load power supply systems that require high voltage stability, I-V droop control may require finer parameter adjustment to maintain system stability. Table 3 shows the advantages and disadvantages of the two droop controls.

Table 3. Comparison of V-I droop control and I-V droop control.

Droop Control	V-I Droop Control	I-V Droop Control
Characteristic	• Voltage is used as the main control variable	• Current is used as the main control variable
Advantages	• Good power distribution characteristics	• Fast response speed
Disadvantages	• Slow response speed • High requirements for control structure design	• Low power distribution accuracy • Relative lack of stability
Application scenarios	• Large-scale systems with high power distribution accuracy requirements	• Small-scale systems with high response speed requirements

5. Conclusions

To reduce the volatility of PV power generation and improve energy utilization efficiency, it is necessary to establish a PV power generation system with ESS. In this paper, ESS is discussed in summary, and HESS is introduced by combining the two key indicators of energy density and power density. Based on the research of many experts and scholars, the Battery-SC HESS was finally selected. Moreover, two kinds of power smoothing control strategies, namely centralized and distributed, were analyzed for HESS power distribution problems, and the advantages and disadvantages of these two control strategies were analyzed and discussed.

It was concluded that the centralized control strategy is suitable for systems requiring unified management of energy storage resources or high control accuracy, such as large-scale centralized PV power stations. The distributed control strategy is suitable for systems with complex topological structures or high real-time response requirements, such as community-distributed PV power generation systems.

In addition, this paper found that most studies only focus on a single control algorithm in a centralized control strategy or a distributed control strategy, and only a small number of scholars try to combine the control algorithms in these two strategies. In the future,

many experts and scholars may combine the advantages of these two strategies to propose more comprehensive control strategies.

Funding: This work was supported in part by the National Natural Science Foundation of China under Grant 52107177 and Grant U22A20226, and in part by the Wuxi University Research Start-up Fund for Introduced Talents under Grant 2024r025.

Conflicts of Interest: Author Fuping Ma was employed by the Chengdu Power Supply Company, State Grid Sichuan Electric Power Company. The remaining authors declare that the research was conducted in the absence of any commercial or financial relationships that could be construed as a potential conflict of interest.

Abbreviations

PV	Photovoltaic
ESS	Energy storage system
HESS	Hybrid energy storage system
MPC	Model predictive control
BES	Battery energy storage
CAES	Compressed-air energy storage
PHES	Pumped hydroelectric energy storage
FC	Fuel cell
SMES	Superconducting magnetic energy storage
FESS	Flywheel energy storage system
SC	Supercapacitor
HES	High energy storage
HPS	High power storage
EMD	Empirical mode decomposition
LPF	Low-pass filter
SOC	State of charge
IMF	Intrinsic mode functions
ANN	Artificial neural network

References

1. Kannan, N.; Vakeesan, D. Solar energy for future world—A review. *Renew. Sustain. Energy Rev.* **2016**, *62*, 1092–1105. [CrossRef]
2. Khan, S.U.D.; Wazeer, I.; Almutairi, Z.; Alanazi, M. Techno-economic analysis of solar photovoltaic powered electrical energy storage (EES) system. *Alex. Eng. J.* **2022**, *61*, 6739–6753. [CrossRef]
3. Zhang, X.; Zhao, X.; Smith, S.; Xu, J.; Yu, X. Review of R&D progress and practical application of the solar photovoltaic/thermal (PV/T) technologies. *Renew. Sustain. Energy Rev.* **2012**, *16*, 599–617.
4. Singh, G.K. Solar power generation by PV (photovoltaic) technology: A review. *Energy* **2013**, *53*, 1–13. [CrossRef]
5. Bocklisch, T. Hybrid energy storage approach for renewable energy applications. *J. Energy Storage* **2016**, *8*, 311–319. [CrossRef]
6. Jing, W.; Lai, C.H.; Ling, D.K.; Wong, W.S.; Wong, M.D. Battery lifetime enhancement via smart hybrid energy storage plug-in module in standalone photovoltaic power system. *J. Energy Storage* **2019**, *21*, 586–598. [CrossRef]
7. Gao, Y.; Cai, Y.; Liu, C. Annual operating characteristics analysis of photovoltaic-energy storage microgrid based on retired lithium iron phosphate batteries. *J. Energy Storage* **2022**, *45*, 103769. [CrossRef]
8. Lei, M.; Yang, Z.; Wang, Y.; Xu, H.; Meng, L.; Vasquez, J.C.; Guerrero, J.M. An MPC-based ESS control method for PV power smoothing applications. *IEEE Trans. Power Electron.* **2017**, *33*, 2136–2144. [CrossRef]
9. Abdalla, A.A.; El Moursi, M.S.; El-Fouly, T.H.; Al Hosani, K.H. A novel adaptive power smoothing approach for PV power plant with hybrid energy storage system. *IEEE Trans. Sustain. Energy* **2023**, *14*, 1457–1473. [CrossRef]
10. Wu, X.; Wu, Y.; Tang, Z.; Kerekes, T. An adaptive power smoothing approach based on artificial potential field for PV plant with hybrid energy storage system. *Sol. Energy* **2024**, *270*, 112377. [CrossRef]
11. Dagar, A.; Gupta, P.; Niranjan, V. Microgrid protection: A comprehensive review. *Renew. Sustain. Energy Rev.* **2021**, *149*, 111401. [CrossRef]
12. Yuan, H.; Ye, H.; Chen, Y.; Deng, W. Research on the optimal configuration of photovoltaic and energy storage in rural microgrid. *Energy Rep.* **2022**, *8*, 1285–1293. [CrossRef]

13. Shuai, Z.; Sun, Y.; Shen, Z.J.; Tian, W.; Tu, C.; Li, Y.; Yin, X. Microgrid stability: Classification and a review. *Renew. Sustain. Energy Rev.* **2016**, *58*, 167–179. [CrossRef]
14. Bullich-Massagué, E.; Cifuentes-García, F.J.; Glenny-Crende, I.; Cheah-Mañé, M.; Aragüés-Peñalba, M.; Díaz-González, F.; Gomis-Bellmunt, O. A review of energy storage technologies for large scale photovoltaic power plants. *Appl. Energy* **2020**, *274*, 115213. [CrossRef]
15. Choudhury, S. Review of energy storage system technologies integration to microgrid: Types, control strategies, issues, and future prospects. *J. Energy Storage* **2022**, *48*, 103966. [CrossRef]
16. Rana, M.M.; Uddin, M.; Sarkar, M.R.; Meraj, S.T.; Shafiullah, G.M.; Muyeen, S.M.; Jamal, T. Applications of energy storage systems in power grids with and without renewable energy integration—A comprehensive review. *J. Energy Storage* **2023**, *68*, 107811. [CrossRef]
17. Sukumar, S.; Marsadek, M.; Agileswari, K.R.; Mokhlis, H. Ramp-rate control smoothing methods to control output power fluctuations from solar photovoltaic (PV) sources—A review. *J. Energy Storage* **2018**, *20*, 218–229. [CrossRef]
18. Rana, M.M.; Uddin, M.; Sarkar, M.R.; Shafiullah, G.M.; Mo, H.; Atef, M. A review on hybrid photovoltaic–Battery energy storage system: Current status, challenges, and future directions. *J. Energy Storage* **2022**, *51*, 104597. [CrossRef]
19. De Siqueira LM, S.; Peng, W. Control strategy to smooth wind power output using battery energy storage system: A review. *J. Energy Storage* **2021**, *35*, 102252. [CrossRef]
20. Luo, J.; Wei, X.; Gao, S.; Huang, T.; Li, D. Summary and outlook of capacity configuration and energy management technology of high-speed railway energy storage system. *Proc. CSEE* **2022**, *42*, 7028–7051.
21. Kang, H.; Jung, S.; Lee, M.; Hong, T. How to better share energy towards a carbon-neutral city? A review on application strategies of battery energy storage system in city. *Renew. Sustain. Energy Rev.* **2022**, *157*, 112113. [CrossRef]
22. May, G.J.; Davidson, A.; Monahov, B. Lead batteries for utility energy storage: A review. *J. Energy Storage* **2018**, *15*, 145–157. [CrossRef]
23. Chen, L.; Zheng, T.; Mei, S.; Xue, X.; Liu, B.; Lu, Q. Review and prospect of compressed air energy storage system. *J. Mod. Power Syst. Clean Energy* **2016**, *4*, 529–541. [CrossRef]
24. Kurşun, B.; Ökten, K. Comprehensive energy, exergy, and economic analysis of the scenario of supplementing pumped thermal energy storage (PTES) with a concentrated photovoltaic thermal system. *Energy Convers. Manag.* **2022**, *260*, 115592. [CrossRef]
25. Pérez-Díaz, J.I.; Chazarra, M.; García-González, J.; Cavazzini, G.; Stoppato, A. Trends and challenges in the operation of pumped-storage hydropower plants. *Renew. Sustain. Energy Rev.* **2015**, *44*, 767–784. [CrossRef]
26. Venkataramani, G.; Parankusam, P.; Ramalingam, V.; Wang, J. A review on compressed air energy storage–A pathway for smart grid and polygeneration. *Renew. Sustain. Energy Rev.* **2016**, *62*, 895–907. [CrossRef]
27. Rehman, S.; Al-Hadhrami, L.M.; Alam, M.M. Pumped hydro energy storage system: A technological review. *Renew. Sustain. Energy Rev.* **2015**, *44*, 586–598. [CrossRef]
28. Gugulothu, R.; Nagu, B.; Pullaguram, D. Energy management strategy for standalone DC microgrid system with photovoltaic/fuel cell/battery storage. *J. Energy Storage* **2023**, *57*, 106274. [CrossRef]
29. Mekhilef, S.; Saidur, R.; Safari, A. Comparative study of different fuel cell technologies. *Renew. Sustain. Energy Rev.* **2012**, *16*, 981–989. [CrossRef]
30. Buckles, W.; Hassenzahl, W.V. Superconducting magnetic energy storage. *IEEE Power Eng. Rev.* **2000**, *20*, 16–20. [CrossRef]
31. Amry, Y.; Elbouchikhi, E.; Le Gall, F.; Ghogho, M.; El Hani, S. Optimal sizing and energy management strategy for EV workplace charging station considering PV and flywheel energy storage system. *J. Energy Storage* **2023**, *62*, 106937. [CrossRef]
32. Faraji, F.; Majazi, A.; Al-Haddad, K. A comprehensive review of flywheel energy storage system technology. *Renew. Sustain. Energy Rev.* **2017**, *67*, 477–490.
33. Arani, A.A.K.; Karami, H.; Gharehpetian, G.B.; Hejazi, M.S.A. Review of Flywheel Energy Storage Systems structures and applications in power systems and microgrids. *Renew. Sustain. Energy Rev.* **2017**, *69*, 9–18. [CrossRef]
34. Ghanaatian, M.; Lotfifard, S. Control of flywheel energy storage systems in the presence of uncertainties. *IEEE Trans. Sustain. Energy* **2018**, *10*, 36–45. [CrossRef]
35. Zhang, L.; Hu, X.; Wang, Z.; Sun, F.; Dorrell, D.G. A review of supercapacitor modeling, estimation, and applications: A control/management perspective. *Renew. Sustain. Energy Rev.* **2018**, *81*, 1868–1878. [CrossRef]
36. Hemmati, R.; Saboori, H. Emergence of hybrid energy storage systems in renewable energy and transport applications–A review. *Renew. Sustain. Energy Rev.* **2016**, *65*, 11–23. [CrossRef]
37. Zimmermann, T.; Keil, P.; Hofmann, M.; Horsche, M.F.; Pichlmaier, S.; Jossen, A. Review of system topologies for hybrid electrical energy storage systems. *J. Energy Storage* **2016**, *8*, 78–90. [CrossRef]
38. Sharma, R.K.; Mishra, S. Dynamic power management and control of a PV PEM fuel-cell-based standalone ac/dc microgrid using hybrid energy storage. *IEEE Trans. Ind. Appl.* **2017**, *54*, 526–538. [CrossRef]
39. Chia, Y.Y.; Lee, L.H.; Shafiabady, N.; Isa, D. A load predictive energy management system for supercapacitor-battery hybrid energy storage system in solar application using the Support Vector Machine. *Appl. Energy* **2015**, *137*, 588–602. [CrossRef]

40. Marzebali, M.H.; Mazidi, M.; Mohiti, M. An adaptive droop-based control strategy for fuel cell-battery hybrid energy storage system to support primary frequency in stand-alone microgrids. *J. Energy Storage* **2020**, *27*, 101127. [CrossRef]
41. Wang, B.; Gao, F.; Stanislawski, R.; Królczyk, G.; Gardoni, P.; Li, Z. Fusion deconvolution for reliability analysis of a flywheel-battery hybrid energy storage system. *J. Energy Storage* **2022**, *49*, 104095. [CrossRef]
42. Li, X.; Palazzolo, A. A review of flywheel energy storage systems: State of the art and opportunities. *J. Energy Storage* **2022**, *46*, 103576. [CrossRef]
43. Li, J.; Yao, F.; Yang, Q.; Wei, Z.; He, H. Variable voltage control of a hybrid energy storage system for firm frequency response in the UK. *IEEE Trans. Ind. Electron.* **2022**, *69*, 13394–13404. [CrossRef]
44. Yang, R.H.; Jin, J.X.; Zhou, Q.; Xiao, M. Non-droop-control-based cascaded superconducting magnetic energy storage/battery hybrid energy storage system. *J. Energy Storage* **2022**, *54*, 105309. [CrossRef]
45. Xu, D.; Liu, Q.; Yan, W.; Yang, W. Adaptive terminal sliding mode control for hybrid energy storage systems of fuel cell, battery and supercapacitor. *Ieee Access* **2019**, *7*, 29295–29303. [CrossRef]
46. Yang, T.; Mok, K.T.; Ho, S.S.; Tan, S.C.; Lee, C.K.; Hui, R.S. Use of integrated photovoltaic-electric spring system as a power balancer in power distribution networks. *IEEE Trans. Power Electron.* **2018**, *34*, 5312–5324. [CrossRef]
47. Devassy, S.; Singh, B. Performance analysis of solar PV array and battery integrated unified power quality conditioner for microgrid systems. *IEEE Trans. Ind. Electron.* **2020**, *68*, 4027–4035. [CrossRef]
48. Khan, A.; D'silva, S.; Fard, A.Y.; Shadmand, M.B.; Abu-Rub, H. On stability of PV clusters with distributed power reserve capability. *IEEE Trans. Ind. Electron.* **2020**, *68*, 3928–3938. [CrossRef]
49. Li, Z.; Chan, K.W.; Hu, J. Adaptive droop control using adaptive virtual impedance for microgrids with variable PV outputs and load demands. *IEEE Trans. Ind. Electron.* **2020**, *68*, 9630–9640. [CrossRef]
50. Shan, Y.; Hu, J.; Liu, M. Model predictive voltage and power control of islanded PV-battery microgrids with washout-filter-based power sharing strategy. *IEEE Trans. Power Electron.* **2019**, *35*, 1227–1238. [CrossRef]
51. Kouchachvili, L.; Yaïci, W.; Entchev, E. Hybrid battery/supercapacitor energy storage system for the electric vehicles. *J. Power Sources* **2018**, *374*, 237–248. [CrossRef]
52. Kotra, S.; Mishra, M.K. Design and stability analysis of DC microgrid with hybrid energy storage system. *IEEE Trans. Sustain. Energy* **2019**, *10*, 1603–1612. [CrossRef]
53. Rocha, L.C.S.; Junior, P.R.; Aquila, G. Multiobjective optimization of hybrid wind-photovoltaic plants with battery energy storage system: Current situation and possible regulatory changes. *J. Energy Storage* **2022**, *51*, 104467. [CrossRef]
54. Diaz-Gonzalez, F.; Chillón-Antón, C.; Llonch-Masachs, M.; Galceran-Arellano, S.; Rull-Duran, J.; Bergas-Jané, J.; Bullich-Massagué, E. A hybrid energy storage solution based on supercapacitors and batteries for the grid integration of utility scale photovoltaic plants. *J. Energy Storage* **2022**, *51*, 104446. [CrossRef]
55. Shaban, M.; Mosa, M.A.; Ali, A.A.; Abdel-Latif, K.M. Effect of power sharing control techniques of hybrid energy storage system during fault conditions in DC microgrid. *J. Energy Storage* **2023**, *72*, 108249. [CrossRef]
56. Li, X.; Hui, D.; Lai, X. Battery energy storage station (BESS)-based smoothing control of photovoltaic (PV) and wind power generation fluctuations. *IEEE Trans. Sustain. Energy* **2013**, *4*, 464–473. [CrossRef]
57. Li, G.; Yang, Z.; Li, B.; Bi, H. Power allocation smoothing strategy for hybrid energy storage system based on Markov decision process. *Appl. Energy* **2019**, *241*, 152–163. [CrossRef]
58. Mahlooji, M.H.; Mohammadi, H.R.; Rahimi, M. A review on modeling and control of grid-connected photovoltaic inverters with LCL filter. *Renew. Sustain. Energy Rev.* **2018**, *81*, 563–578. [CrossRef]
59. Jiao, Y.; Månsson, D. Study of the oversized capacity and the increased energy loss of hybrid energy storage systems and design of an improved controller based on the low-pass filter. *J. Energy Storage* **2022**, *50*, 104241. [CrossRef]
60. Roy, P.K.S.; Karayaka, H.B.; Yan, Y. Investigations into best cost battery-supercapacitor hybrid energy storage system for a utility scale PV array. *J. Energy Storage* **2019**, *22*, 50–59. [CrossRef]
61. Pigazo, A.; Liserre, M.; Mastromauro, R.A.; Moreno, V.M.; Dell'Aquila, A. Wavelet-based islanding detection in grid-connected PV systems. *IEEE Trans. Ind. Electron.* **2008**, *56*, 4445–4455. [CrossRef]
62. Lamsal, D.; Sreeram, V.; Mishra, Y.; Kumar, D. Output power smoothing control approaches for wind and photovoltaic generation systems: A review. *Renew. Sustain. Energy Rev.* **2019**, *113*, 109245. [CrossRef]
63. Ma, W.; Gao, H.; Zhang, Y.; Peng, F. Adaptive PCC power fluctuation smoothing method based on EWT for distributed PV-energy storage. *Power Syst. Prot. Control* **2024**, *52*, 51–61.
64. Yin, Y.; Yu, Z.; Gou, X.; Wang, J. Photovoltaic power prediction model based on empirical mode decomposition-long-short memory neural network. In Proceedings of the 2021 International Conference on Intelligent Computing, Automation and Systems (ICICAS), Chongqing, China, 29–31 December 2021; pp. 349–353.
65. Zheng, H.; Xie, L.; Ye, L.; Lu, P.; Wang, K.F. Hybrid energy storage smoothing output fluctuation strategy considering photovoltaic dual evaluation indicators. *Trans. China Electrotech. Soc.* **2021**, *36*, 1805–1817.

66. Kim, T.; Moon, H.; Kwon, D.; Moon, S.I. A smoothing method for wind power fluctuation using hybrid energy storage. In Proceedings of the 2015 IEEE Power and Energy Conference at Illinois (PECI), Champaign, IL, USA, 20–21 February 2015; pp. 1–6.
67. Kini, R.; Raker, D.; Stuart, T.; Ellingson, R.; Heben, M.; Khanna, R. Mitigation of PV variability using adaptive moving average control. *IEEE Trans. Sustain. Energy* **2019**, *11*, 2252–2262. [CrossRef]
68. Tian, B.; Zhang, Z.; Yang, M. Research on hybrid energy storage power allocation and capacity determination based on multiple moving average filtering. *Trans. China Electrotech. Soc.* **2024**, *39*, 1548–1564.
69. Adeyemo, A.A.; Amusan, O.T. Modelling and multi-objective optimization of hybrid energy storage solution for photovoltaic powered off-grid net zero energy building. *J. Energy Storage* **2022**, *55*, 105273. [CrossRef]
70. Medghalchi, Z.; Taylan, O. A novel hybrid optimization framework for sizing renewable energy systems integrated with energy storage systems with solar photovoltaics, wind, battery and electrolyzer-fuel cell. *Energy Convers. Manag.* **2023**, *294*, 117594. [CrossRef]
71. Liu, Y.; Liu, X.; Li, X.; Yuan, H.; Xue, Y. Model predictive control-based dual-mode operation of an energy-stored quasi-Z-source photovoltaic power system. *IEEE Trans. Ind. Electron.* **2022**, *70*, 9169–9180. [CrossRef]
72. Wang, T.; Kamath, H.; Willard, S. Control and optimization of grid-tied photovoltaic storage systems using model predictive control. *IEEE Trans. Smart Grid* **2014**, *5*, 1010–1017. [CrossRef]
73. Hredzak, B.; Agelidis, V.G.; Jang, M. A model predictive control system for a hybrid battery-ultracapacitor power source. *IEEE Trans. Power Electron.* **2013**, *29*, 1469–1479. [CrossRef]
74. Garcia-Torres, F.; Bordons, C. Optimal economical schedule of hydrogen-based microgrids with hybrid storage using model predictive control. *IEEE Trans. Ind. Electron.* **2015**, *62*, 5195–5207. [CrossRef]
75. Zeng, P.P.; Wu, Z.; Zhang, X.P.; Liang, C.; Zhang, Y. Model predictive control for energy storage systems in a network with high penetration of renewable energy and limited export capacity. In Proceedings of the 2014 Power Systems Computation Conference, Wroclaw, Poland, 18–22 August 2014; pp. 1–7.
76. Sun, Y.; Li, S.; Lin, B. Artificial neural network for control and grid integration of residential solar photovoltaic systems. *IEEE Trans. Sustain. Energy* **2017**, *8*, 1484–1495. [CrossRef]
77. Ramoul, J.; Chemali, E.; Dorn-Gomba, L. A neural network energy management controller applied to a hybrid energy storage system using multi-source inverter. In Proceedings of the 2018 IEEE Energy Conversion Congress and Exposition (ECCE), Portland, OR, USA, 23–27 September 2018; pp. 2741–2747.
78. Errouha, M.; Derouich, A.; Motahhir, S. Optimization and control of water pumping PV systems using fuzzy logic controller. *Energy Rep.* **2019**, *5*, 853–865. [CrossRef]
79. Cohen, I.J.; Wetz, D.A.; McRee, B.J. Fuzzy logic control of a hybrid energy storage module for use as a high rate prime power supply. *IEEE Trans. Dielectr. Electr. Insul.* **2017**, *24*, 3887–3893. [CrossRef]
80. Feng, X.; Gooi, H.B.; Chen, S.X. Hybrid energy storage with multimode fuzzy power allocator for PV systems. *IEEE Trans. Sustain. Energy* **2014**, *5*, 389–397. [CrossRef]
81. Jiang, W.; Fahimi, B. Multiport power electronic interface—Concept, modeling, and design. *IEEE Trans. Power Electron.* **2010**, *26*, 1890–1900. [CrossRef]
82. de Doile, G.N.D.; Junior, P.R.; Rocha, L.C.S.; Rocha, L.C.S.; Janda, K.; Aquila, G.; Peruchi, R.S.; Balestrassi, P.P. Feasibility of hybrid wind and photovoltaic distributed generation and battery energy storage systems under techno-economic regulation. *Renew. Energy* **2022**, *195*, 1310–1323. [CrossRef]
83. Tayab, U.B.; Roslan, M.A.B.; Hwai, L.J.; Kashif, M. A review of droop control techniques for microgrid. *Renew. Sustain. Energy Rev.* **2017**, *76*, 717–727. [CrossRef]
84. Xu, Q.; Xiao, J.; Wang, P.; Pan, X.; Wen, C. A decentralized control strategy for autonomous transient power sharing and state-of-charge recovery in hybrid energy storage systems. *IEEE Trans. Sustain. Energy* **2017**, *8*, 1443–1452. [CrossRef]
85. Xu, Q.; Hu, X.; Wang, P.; Xiao, J.; Tu, P.; Wen, C.; Lee, M.Y. A decentralized dynamic power sharing strategy for hybrid energy storage system in autonomous DC microgrid. *IEEE Trans. Ind. Electron.* **2016**, *64*, 5930–5941. [CrossRef]
86. Xu, Q.; Xiao, J.; Hu, X.; Wang, P.; Lee, M.Y. A decentralized power management strategy for hybrid energy storage system with autonomous bus voltage restoration and state-of-charge recovery. *IEEE Trans. Ind. Electron.* **2017**, *64*, 7098–7108. [CrossRef]
87. Lin, P.; Wang, P.; Xiao, J. An integral droop for transient power allocation and output impedance shaping of hybrid energy storage system in DC microgrid. *IEEE Trans. Power Electron.* **2017**, *33*, 6262–6277. [CrossRef]
88. Zhang, Y.; Li, Y.W. Energy management strategy for supercapacitor in droop-controlled DC microgrid using virtual impedance. *IEEE Trans. Power Electron.* **2016**, *32*, 2704–2716. [CrossRef]
89. Gao, F.; Bozhko, S.; Costabeber, A. Comparative stability analysis of droop control approaches in voltage-source-converter-based DC microgrids. *IEEE Trans. Power Electron.* **2016**, *32*, 2395–2415. [CrossRef]
90. Wang, Z.; Wang, P.; Jiang, W. A decentralized automatic load power allocation strategy for hybrid energy storage system. *IEEE Trans. Energy Convers.* **2020**, *36*, 2227–2238. [CrossRef]

91. Gu, Y.; Li, W.; He, X. Frequency-coordinating virtual impedance for autonomous power management of DC microgrid. *IEEE Trans. Power Electron.* **2014**, *30*, 2328–2337. [CrossRef]
92. Gu, Y.; Xiang, X.; Li, W. Mode-adaptive decentralized control for renewable DC microgrid with enhanced reliability and flexibility. *IEEE Trans. Power Electron.* **2013**, *29*, 5072–5080. [CrossRef]
93. Su, J.; Li, K.; Zhang, L. A decentralized power allocation strategy for dynamically forming multiple hybrid energy storage systems aided with power buffer. *IEEE Trans. Sustain. Energy* **2023**, *14*, 1714–1724. [CrossRef]
94. Wang, H.; Han, M.; Han, R.; Guerrero, J.M.; Vasquez, J.C. A decentralized current-sharing controller endows fast transient response to parallel DC–DC converters. *IEEE Trans. Power Electron.* **2017**, *33*, 4362–4372. [CrossRef]
95. Wandhare, R.G.; Agarwal, V. Novel stability enhancing control strategy for centralized PV-grid systems for smart grid applications. *IEEE Trans. Smart Grid* **2014**, *5*, 1389–1396. [CrossRef]
96. Jena, C.J.; Ray, P.K. Power allocation scheme for grid interactive microgrid with hybrid energy storage system using model predictive control. *J. Energy Storage* **2024**, *81*, 110401. [CrossRef]
97. Sun, C.; Joos, G.; Ali, S.Q.; Paquin, J.N.; Rangel, C.M.; Al Jajeh, F.; Bouffard, F. Design and real-time implementation of a centralized microgrid control system with rule-based dispatch and seamless transition function. *IEEE Trans. Ind. Appl.* **2020**, *56*, 3168–3177. [CrossRef]
98. Cheng, Z.; Li, Z.; Liang, J.; Si, J.; Dong, L.; Gao, J. Distributed coordination control strategy for multiple residential solar PV systems in distribution networks. *Int. J. Electr. Power Energy Syst.* **2020**, *117*, 105660. [CrossRef]
99. Sun, K.; Zhang, L.; Xing, Y.; Guerrero, J.M. A distributed control strategy based on DC bus signaling for modular photovoltaic generation systems with battery energy storage. *IEEE Trans. Power Electron.* **2011**, *26*, 3032–3045. [CrossRef]
100. Pegueroles-Queralt, J.; Bianchi, F.D.; Gomis-Bellmunt, O. A power smoothing system based on supercapacitors for renewable distributed generation. *IEEE Trans. Ind. Electron.* **2014**, *62*, 343–350. [CrossRef]
101. Cai, H.; Xiang, J.; Wei, W.; Chen, M.Z. V-dp/dv Droop Control for PV Sources in DC Microgrids. *IEEE Trans. Power Electron.* **2017**, *33*, 7708–7720. [CrossRef]